PHILOSOPHICAL MAGAZINE B, 1999, VOL. 79, NO. 11/12, 2091–2102

Low frequency dynamics of silica xerogel porous system

G. CICOGNANI†, A. J. DIANOUX‡, A. FONTANA§‖, F. ROSSI§, M. MONTAGNA§, T. SCOPIGNO§, J. PELOUS¶, F. TERKI¶, J. N. PILLIEZ¶ and T. WOIGNIER¶

† Institut Laue Langevin, BP 156, F-38042 Grenoble Cedex 9, France and Istituto Nazionale per la Fisica della Materia, Italy
‡ Institut Laue Langevin, BP 156, F-38042 Grenoble Cedex 9, France
§ Dipartimento di Fisica and Istituto Nazionale di Fisica della Materia, Universita' di Trento, I-38050 Povo(Trento), Italy
¶ Laboratoire des Verres, UMR5587, Universite Montpellier II, Place Eugene Bataillon, case 069, 34095 Montpellier Cedex, France

ABSTRACT

Coherent inelastic neutron and light (Raman and Brillouin) scattering measurements are reported on silica xerogels over a wide range of densities and temperatures. Raman scattering results show the presence of a boson peak at temperatures where the quasielastic contribution is negligible. The boson peak of xerogels is at a frequency around 35 cm^{-1} and has a shape similar to that of melted silica. At lower frequencies (7–16 cm^{-1}) another bump is visible in the Raman scattering, believed to be connected to the presence of the pores and its frequency connected to their mean sizes. This important result seems to indicate that the disorder introduced by the presence of the pores does not influence very much the density of states in the frequency range of the boson peak. A comparison is made between the Q dependence of the elastic and inelastic structure factors as a function of sample density and temperature. The absence of a peak in the inelastic structure factor for the Q value corresponding to the first sharp diffraction peak demonstrates the existence of random-phase modes for energies around the boson peak.

§ 1. INTRODUCTION

Extensive research performed over the last two decades on different aspects of the glassy state has established a number of peculiar properties that are strikingly different from those of the respective crystalline solids, and are being commonly referred to as universal for disordered systems (Phillips 1981, Fontana and Viliani 1998). Some of these effects concern low energy dynamics and manifest themselves in low temperature specific heat, thermal conductivity, and inelastic scattering experiments. An important conceptual result argued by the low energy behaviour is that disordered systems support, in addition to Debye-like phonons (non-dispersive thermal plane waves), some other excess vibrational modes. The lowest energy excitations (corresponding to $T < 1$ K) can be described successfully in terms of two-level systems (TLSs), coexisting and interacting with Debye phonons. However, at higher temperatures, effects are observed that this TLS model cannot account for. Above 1 K the thermal conductivity reaches a plateau, while the specific heat exhibits a

‖ Author for correspondence. E-mail: afontana@science.unitn.it

Philosophical Magazine B ISSN 0141–8637 print/ISSN 1463–6417 online
http://www.tandf.co.uk/JNLS/phb.htm
http://www.taylorandfrancis.com/JNLS/phb.htm

further excess over that predicted by the standard Debye model, which is manifested in a bump in a C_p/T^3 versus T plot (Phillips 1981). The corresponding total vibrational density of states (VDOS) $g(\omega)$, deduced from inelastic neutron scattering measurements, exhibits a broad maximum in a $g(\omega)/\omega^2$ versus ω plot, named boson peak (BP), again indicating non-Debye behaviour (Buchenau *et al.* 1986, 1988, Brodin *et al.* 1994, Carini *et al.* 1995). The excitations responsible have been proved to be essentially harmonic by a number of inelastic scattering and infrared experiments, thus confirming that TLSs alone cannot account for the anomalous properties. In some models the enhancement of $g(\omega)$ in the frequency range above $10\,cm^{-1}$ is explained as phonon localization due to strong scattering of phonons with wavelengths comparable to the length scale of the static density fluctuations, i.e., 5–50 Å (Mariotto *et al.* 1988, Fontana and Viliani 1995) or as localized low frequency resonant modes as soft modes (Karpov and Parshin 1985). An alternative interpretation is that the vibrational states are collective propagating modes in 'excess' of the Debye prediction (Masciovecchio *et al.* 1999). In a topological disordered system the eigenvectors of the modes cannot be pure plane waves. The eigenvectors can be decomposed on plane waves plus a random part, which remembers a white noise in the atomic displacements, and this could give rise to the observed increase of states at low energy (Fontana *et al.* 1999a). Information on the character of the vibrations contributing to the BP can be inferred by comparing different spectroscopic experimental techniques. However, while low temperature specific heat and inelastic neutron scattering measurements yield rather unambiguous data for the total density of states, optical scattering data are affected by the efficiency of the photon-to-vibration coupling (Brodin *et al.* 1994). In particular, first-order Raman scattering in disordered systems is expressed by the vibrational density of states modulated by the coupling function $C(\omega)$. The available experimental data based on the direct comparison of Raman spectra with neutron scattering and low temperature specific heat strongly suggest that for melt quenched glasses, the coupling function is a smooth varying function, almost linear in the BP frequency region (Fontana 1987, 1990, Sokolov *et al.* 1993). The broad band observed in glasses in the range $20–100\,cm^{-1}$ in the Raman scattering is then identified with the corresponding bump in the $g(\omega)/\omega^2$ frequency dependence.

At lower frequencies (less than $20\,cm^{-1}$) Raman and neutron scattering show another characteristic feature, quasielastic scattering (QES), which usually is attributed to relaxation processes, as it is centred around zero frequency (Lorentzian-like shape) and increases in intensity with temperature at a higher rate than the Bose population factor (Carini *et al.* 1995). The microscopic origin of QES could be the same the one that is at the origin of the acoustic attenuation peak which occurs above 20 K in glasses (Phillips 1981). Application of this model has provided a successful interpretation of Raman scattering data in vitreous silica and in B_2O_3, but was unable to describe quantitatively experimental results in borate and phosphate glasses (Carini *et al.* 1995). Another possible interpretation of QES has been achieved in terms of two-phonon scattering. However, an unambiguous interpretation of this scattering is not yet feasible.

The vibrational dynamics of the glassy state have a close relationship to its atomic scale structure and to its mechanical and thermal properties (Fontana *et al.* 1997). In this regard we have studied silica xerogel systems, since they can be produced at different macroscopic densities over an exceptionally wide range (Fontana *et al.* 1999b,c). The mean size of macropores l_p changes from $l_p \sim 30\,nm$

($\rho \approx 0.5\,\mathrm{g\,cm^{-3}}$) to $l_p \approx 10\,\mathrm{nm}$ ($\rho \approx 1.73\,\mathrm{g\,cm^{-3}}$) (Dieudonne–George 1998). The microscopic density of the solid phase between the pores is close to $\rho \approx 2.2\,\mathrm{g\,cm^{-3}}$, the same as melt quenched vitreous silica (Dieudonne–George 1998), although the presence of micropores inside the solid phase cannot be excluded.

In this work we compare the results of neutron and inelastic light (Brillouin and Raman) scattering performed on these xerogels at different temperatures (300–750 K) and with melt quenched vitreous silica ($2.2\,\mathrm{g\,cm^{-3}}$). In the low frequency part of the neutron and Raman spectra, the BP, characteristic of glasses, is observed at all densities at high temperatures where the quasielastic contribution tends to be negligible. The nature of the vibrations at the BP frequency is studied by the Q dependence of the dynamic structure factor $S(Q, \omega_{BP})$ of neutron scattering.

§ 2. Samples and experimental technique

Alcogel samples were prepared by hydrolysis and polycondensation reactions of tetraethoxysilanol dissolved in methanol (Brinker and Scherer 1990). The alcogel is aged at 200°C in an autoclave for 12 h at 4 MPa. The ageing favours the gel syneresis dissolution–redeposition of the silica. As a function of the network stiffening, the drying shrinkage can be controlled and it is possible to synthesize sol–gel with a bulk density in the range 0.5–$1.73\,\mathrm{g\,cm^{-3}}$. Xerogels have large surface area, the surface being covered by dangling SiOH bonds. The porous structure easily absorbs H_2O molecules, which can be bonded to the surface (chemical water) or can fill the pores (physical water) (Fontana *et al.* 1999b). The samples were heat treated at 600°C for 24 h to eliminate most of the adsorbed impurities and water.

The inelastic neutron scattering results were obtained at the IN6 time-of-flight spectrometer of the Institut Laue-Langevin, Grenoble, using a neutron incident wavelength of 5.12 Å (3.12 meV); the instrument elastic resolution was about 0.1 meV. Raman scattering experiments were performed using a standard experimental setup over a wide frequency range (5–$5000\,\mathrm{cm^{-1}}$). Brillouin spectra were taken using a multipass interferometer in back-scattering configuration; the free spectral range was chosen between 15 GHz to 75 GHz depending on the sample density, and the finess was 70.

The first-order scattering both for Raman scattering or inelastic neutron scattering is connected to the vibrational density of states by (Galenneer and Sen, 1978, Price and Carpenter 1987):

$$I_{R,N}(\omega, T) \propto C_{R,N}(\omega)\, g(\omega)\, [n(\omega, T) + 1]/\omega, \tag{1}$$

where $g(\omega)$ is an effective density of states, $n(\omega, T)$ is the Bose population factor, and $C_{RN(\omega)}$ is the probe–excitations coupling function. Since neutrons feel the absolute motion of atoms in space, $C_N(\omega) = 1$. In this paper we report also the Raman and neutron spectral intensity:

$$J_{R,N}(\omega, T) \propto I_{R,N}(\omega, T)/\{[n(\omega, T) + 1]\omega\} \tag{2}$$

which, according to equation (1), corresponds to $C_{R,N}(\omega)\, g(\omega)/\omega^2$.

The standard procedure for obtaining the density of state $g(\omega)$ is the following. In the incoherent approximation, one writes the neutron differential scattering cross-section as

$$d^2\sigma/d\Omega\, d\omega = (k/k_0)\, b^2 \exp(-\hbar\omega/2k_BT)\, S_s(Q, \omega). \tag{3}$$

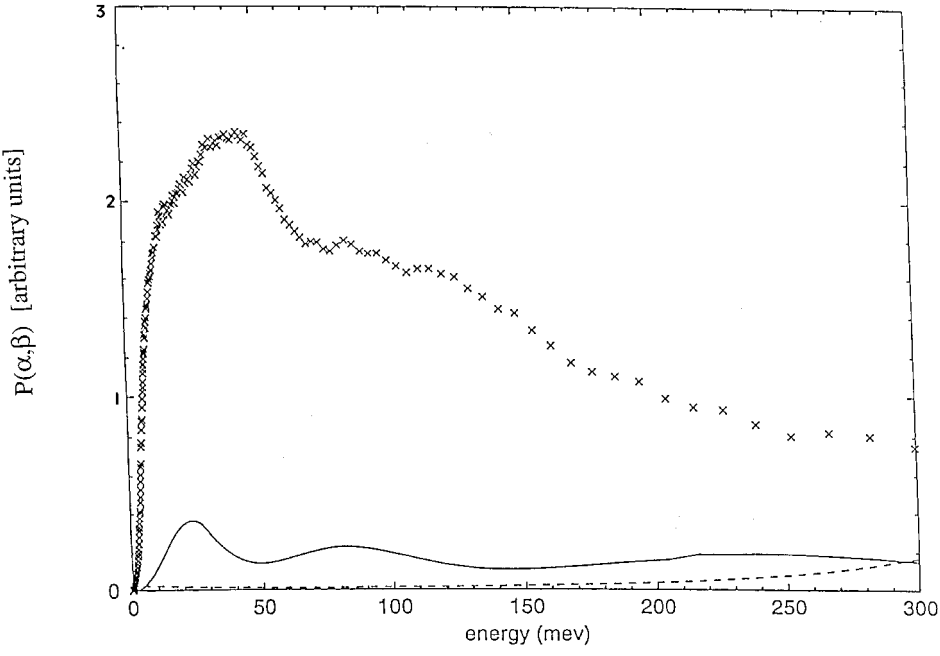

Figure 1. Experimental $P(\alpha, \beta)$ (crosses) at 750 K for the xerogel with $\rho = 1.4\,\mathrm{g\,cm^{-3}}$, with the multiphonon (continous line) and background (broken line) contributions.

It is determined after the usual data correction procedure, such as the subtraction of the empty cell contribution and normalization to a vanadium scan. In the formula, k_0 and k are the incident and scattered neutron wavevectors, b is the scattering length, and $S_s(Q, \omega)$ is the symmetrized scattering law, which is directly related to the $g(\omega)$. Using the reduced variables $\alpha = \hbar^2 Q^2 / 2M k_B T$ and $\beta = \hbar\omega / k_B T$, the scattering law may be written:

$$S_s(\alpha, \beta) = \exp(-Q^2\langle u^2\rangle)[\alpha / 2\beta \sinh(\beta/2)]\, g(\omega). \quad (4)$$

The elastic contribution was identified and subtracted, and the generalized frequency distribution $P(\alpha, \beta)$ was then calculated:

$$P(\alpha, \beta) = 2\beta \sinh(\beta/2)\, S_s(\alpha, \beta)/\alpha = g(\omega) \exp(-Q^2\langle u^2\rangle). \quad (5)$$

The multiphonon contribution and background were estimated and subtracted from the experimental $P(\alpha, \beta)$, as indicated in figure 1. Finally, $g(\omega)$ was extracted from the corrected $P(\alpha, \beta)$, by dividing by the calculated Debye–Waller factor (Fontana *et al.* 1990).

§ 3. Results and discussion

3.1. *Inelastic light and neutron scattering data*

Silica xerogels present quite strong low frequency Raman scattering (Fontana *et al.* 1999b); however the nature of this scattering seems to be different from that of QES in melt quenched glasses. In particular the intensity of QES depends strongly on the thermal history. The origin of the QES is shown by the Raman results of figure 2,

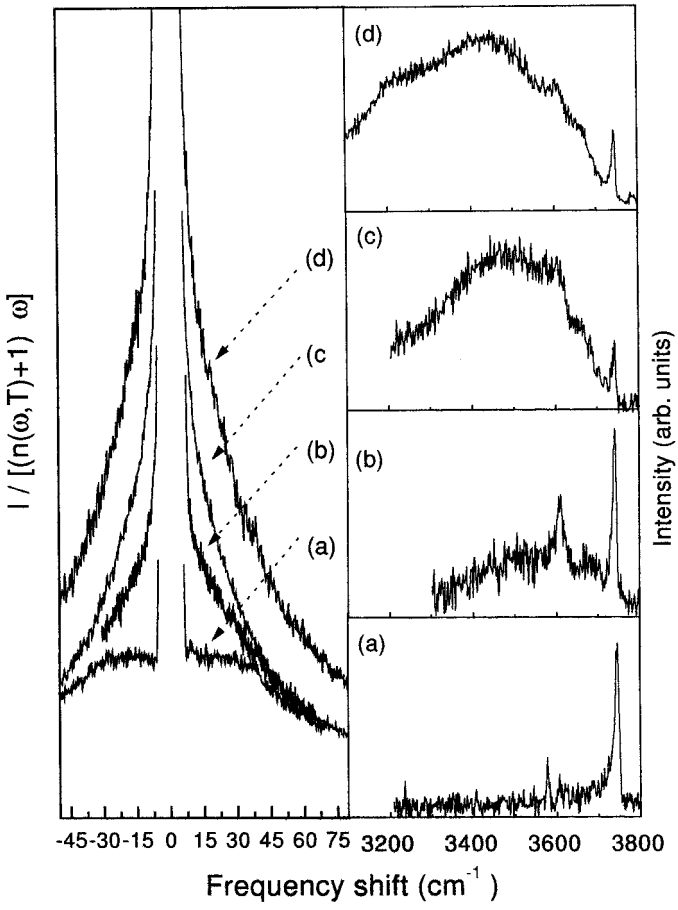

Figure 2. Raman spectral intensity at room temperature for the xerogel with $\rho = 1.73\,g\,cm^{-3}$: (*a*) after annealing at 750 K; (*b*) after ageing for 4 h; (*c*) after ageing for 24 h (this measure was at 400 K); and (*d*) after ageing for 48 h.

taken at room temperature at different steps of thermal history. The broad band centred at about $3500\,cm^{-1}$ is due to the OH stretching vibration of water. After annealing at high temperature it disappears and the sharp peak at about $3740\,cm^{-1}$ of the OH stretching of the free silanol group at the pore surface dominates the spectrum (Armellini *et al.* 1998).

Under the same conditions the intensity of QES is strongly reduced, as shown in figure 2 (*a*). Nevertheless a strong QES remains in the spectrum after the heat treatment at high temperatures. From this experiment it is not clear if it is due to the presence of water inside the micropores of the solid phase of xerogels or to other excitations characteristic of xerogels already found in the aerogels. Anyway, ageing in air at room temperature restores the broad band and the intensity of the QES increases (as shown in figure 2 (*b–d*). It is evident, from these results that QES in these xerogels can be attributed mainly to the presence of water inside the pores (Fontana *et al.* 1999b). Moreover, we have observed that at high temperatures the intensity of this QES is reduced strongly, so these experiments allow us to observe the BP in Raman spectra in xerogels with high density. The Raman scattering spectra

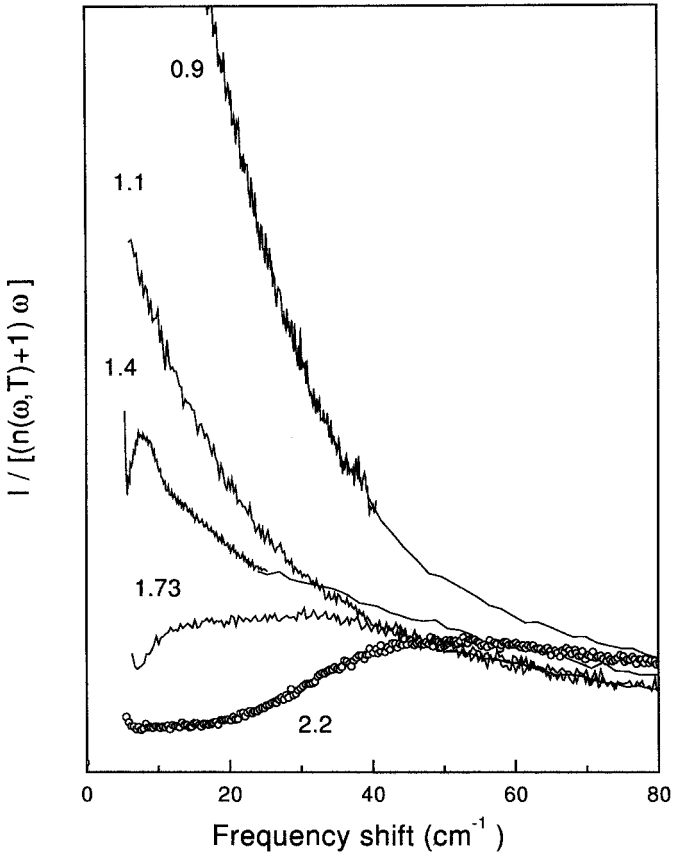

Figure 3. Raman spectral intensity at 750 K on xerogels with $\rho = 0.9\,g\,cm^{-3}$, $\rho = 1.1\,g\,cm^{-3}$, $\rho = 1.4\,g\,cm^{-3}$, $\rho = 1.73\,g\,cm^{-3}$, and $\rho = 2.2\,g\,cm^{-3}$ (melt quenched vitreous silica).

are shown in figure 3 for the four xerogel densities and compared with that of vitreous silica. The spectra were normalized in the region of high frequency optical modes.

Let us focus our attention on the sample with $\rho = 1.73\,g\,cm^{-3}$. The BP maximum frequency is at about $33\,cm^{-1}$, but a new (with respect to melt quenched vitreous silica) bump at about $16\,cm^{-1}$ is evident also. With decreasing sample density the intensity of the low frequency bump increases strongly and shifts at about $8\,cm^{-1}$. Below $\rho = 1.4\,g\,cm^{-3}$ it is no longer possible to measure the position of this bump. We tentatively assign this peak to the dynamics due to the presence of pores: the pore peak.

In figure 4 (*a*) we report the neutron spectral function $J(\omega)$ (see equation (2)) in xerogel with $\rho = 1.4\,g\,cm^{-3}$ at different temperatures. The spectra show the two characteristic features, i.e., the QES and BP. The intensity of QES decreases with increasing temperature, with evidence the presence of the BP at 750 K. The temperature behaviour of QES, as measured by neutron scattering, is similar to that measured by Raman scattering and has the same physical origin as previously discussed. The highest temperature spectrum has the BP maximum frequency at about 5 meV ($40\,cm^{-1}$). Figure 4 (*b*) shows the neutron spectral function in melt quenched vitreous silica ($\rho = 2.2\,g\,cm^{-3}$) at similar temperatures. The QES of vitreous silica is negligible with respect to that of xerogels. The BP has a similar spectral shape in the two

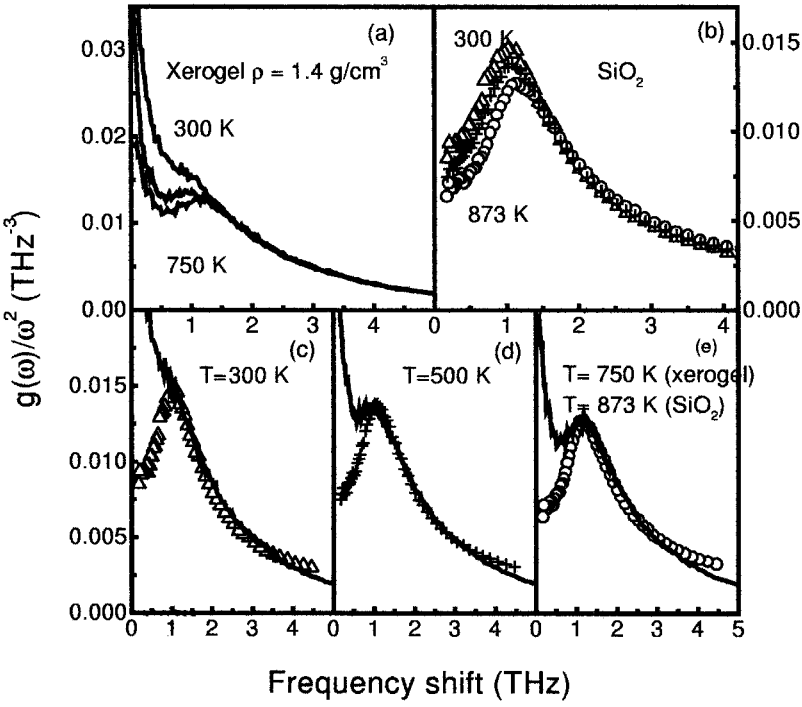

Figure 4. Neutron spectral intensity: (*a*) on xerogel with $\rho = 1.4\,\mathrm{g\,cm^{-3}}$ at 300 K, 500 K, and 750 K; (*b*) on vitreous silica at 300 K, 500 K, and 873 K; (*c*, *d*, *e*) on xerogel with $\rho = 1.4\,\mathrm{g\,cm^{-3}}$ and vitreous silica at different temperatures.

systems. Moreover, the frequency of the maximum shifts with the same rate over the temperature range investigated and has the same intensity (data are given in absolute units), as shown in figure 4 (*c–e*). This behaviour is confirmed at all measured densities as shown in figure 5, where we report the neutron spectral function at 750 K for $\rho = 0.8\,\mathrm{g\,cm^{-3}}$, $\rho = 1.4\,\mathrm{g\,cm^{-3}}$, $\rho = 1.73\,\mathrm{g\,cm^{-3}}$, and in vitreous silica at 853 K ($\rho = 2.2\,\mathrm{g\,cm^{-3}}$).

The frequency of the maximum of the BP is the same in the limit of experimental errors and displacements due to the presence of QES. These experimental results indicate that the vibrational dynamics of the xerogels are more or less the same as those of melt quenched amorphous silica in this frequency range.

Regarding the low frequency region ($\omega < 30\,\mathrm{cm^{-1}}$), both Raman and neutron data show intense scattering, but the pore peak, observed in Raman spectra, is not present in the neutron data. Anyway an intense spectral density of states $g(\omega)/\omega^2$ is expected for low density xerogels because of the very low sound velocities (Fontana *et al.* 1999b) and of the corresponding high Debye density of states (Fontana *et al.* 1999c). In fact this explains the intense low frequency neutron scattering, which increases with the density (figure 4), even if we cannot exclude that an important contribution could arise from the residual water content.

The absence of the pore peak in neutron data indicates that the density of states changes smoothly, passing from the low frequency region of the acoustic modes to the intermediate region of the vibrational modes with wavelength comparable with the pore size. Therefore the peak at 8–16 $\mathrm{cm^{-1}}$ in the Raman spectra seems to be due

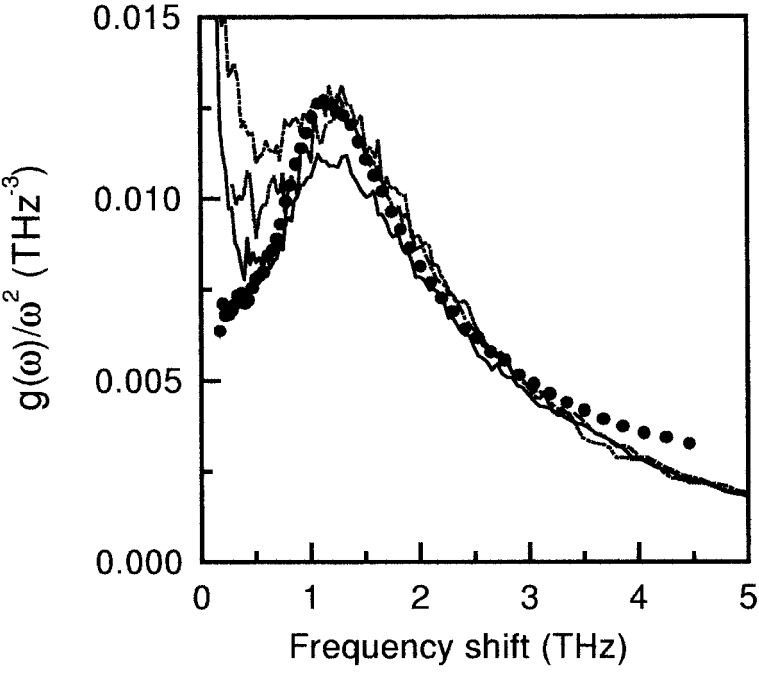

Figure 5. Neutron spectral intensity for xerogels at 750 K, with $\rho = 0.8\,\mathrm{g\,cm^{-3}}$ (full line), $\rho = 1.4\,\mathrm{g\,cm^{-3}}$ (dot-dashed line), $\rho = 1.73\,\mathrm{g\,cm^{-3}}$ (dotted line), and for vitreous silica at 873 K, $\rho = 2.2\,\mathrm{g\,cm^{-3}}$ (circles). Neutron data on vitreous silica are from. Wischnewski *et al.* (1998).

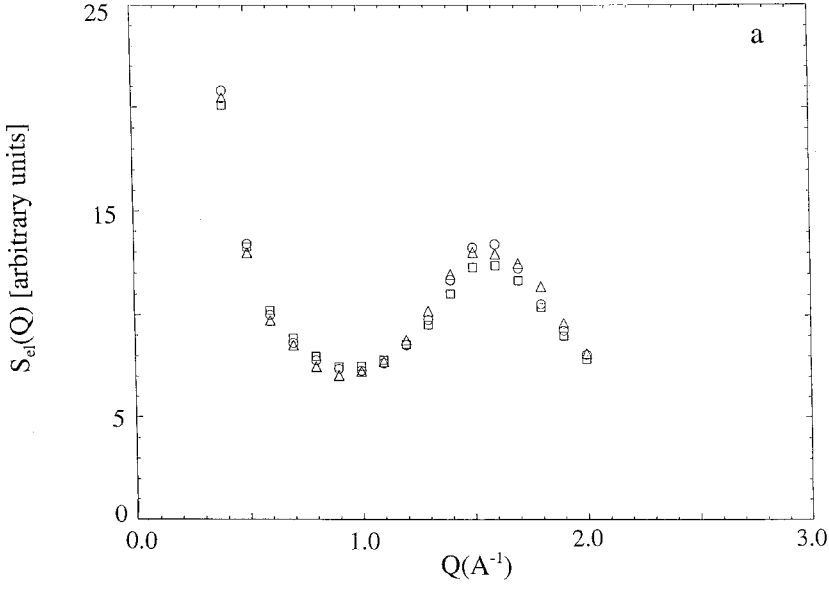

Figure 6. Density dependence of the elastic and inelastic structure factors at 300 K: (*a*) elastic, $\rho = 0.8\,\mathrm{g\,cm^{-3}}$ (circles), $\rho = 1.4\,\mathrm{g\,cm^{-3}}$ (squares), $\rho = 1.73\,\mathrm{g\,cm^{-3}}$ (triangles); (*b*) inelastic in the 4–6 meV range, same symbols as in (*a*); (*c*) inelastic in the 0.5–1.5 meV range, same symbols as in (*a*). The full line is $Q^2 S_{el}(Q)$ (arbitrarily scaled).

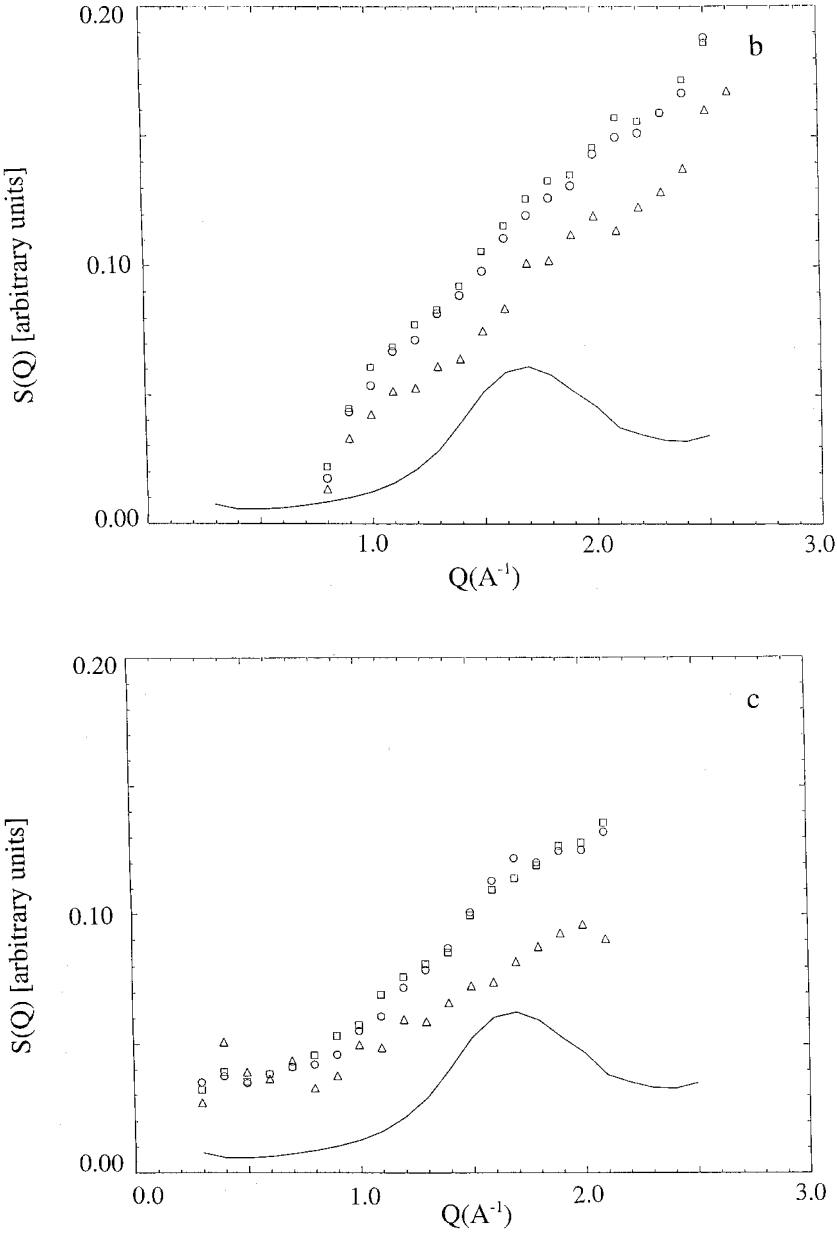

to a strong increases of the Raman coupling function $C(\omega)$ in the crossover frequency region (Fontana *et al.* 1999c).

3.2. *Q dependence of the dynamic structure factor*

Further information on the low frequency vibrational dynamics can be obtained from measuring the dynamic structure factor, as shown in figure 6. It should be mentioned that, due to the dynamic range measured by the present experiment and permitted by the kinematics restriction, the dynamic structure factor $S(Q,\omega)$ is

measured at high Q's ($Q \gg \omega/v_s$, where v_s is the velocity of sound) and should be distinguished from the usual structure factor determined by the direct Brillouin experiments. Anyway, the Q dependence of neutron scattering, represents an important source of additional information. The inelastic structure factor $S(Q,\omega)$ is given by

$$S(Q,\omega) = \left| \sum_j b_j \exp(-W_j) \exp(i\mathbf{Q}\mathbf{R}_j) \mathbf{Q}\mathbf{u}_j / M_j \right|^2, \qquad (6)$$

where the sum is over the N atoms in the vibrating entity, b_j is the neutron scattering length, R_j the position vector, M_j the mass and $\mathbf{u}_j$ the displacement vector of atom j. It is worth noting that the main contribution to $S(Q,\omega)$ for our samples comes, in the case of neutron scattering, from the vibrations of oxygen atoms, because the oxygen neutron cross-section is approximately twice that of silicon.

The inelastic structure factor $S_{\Delta\omega}(Q)$ was calculated by integrating over ω at constant Q the $S(Q,\omega)$ data. The ranges of integration $\Delta\omega$ were taken from 4 meV to 6 meV (around the BP), from 0.5 meV to 1.5 meV (lower frequencies than the BP) and -0.5 meV to $+0.5$ meV (in this last frequency range $S_{\Delta\omega}(Q)$ is the elastic one, and in the following we indicate it as $S_{el}(Q)$). The investigated Q range is limited by the neutron incident wavelength used. Figure 6(*a*) compares the elastic structure factor of different samples, in arbitrary units, and normalized to each other: clearly there is no strong density dependence of the shape of $S_{el}(Q)$.

Figure 6(*b*, *c*) compares the inelastic intensities, normalized with the same factor used for $S_{el}(Q)$, in the frequency region of the BP (figure 6(*b*)) and in a lower frequency region (figure 6(*c*)). While in both regions the inelastic $S_{\Delta\omega}(Q)$ is practically the same for the 0.8 g cm^{-3} and 1.4 g cm^{-3} xerogels, clearly that of the 1.73 g cm^{-3} xerogel deviates from the other two samples.

We observe also that, at very low Q, $S_{\Delta\omega}(Q)$ tends to a larger value (different from zero) in the low frequency range. This fact seems to indicate that multiple scattering effects are larger in that region. Moreover, we can see that the shape of the curves in the lower energy-range (figure 6(*c*)) is different from that obtained in the BP region (figure 6(*b*)), revealing a small angle effect which could be related to peculiar excitations due to the pore structure. The slight tendency to increase at low Q seen on figure 6(*c*) seems to be connected to the large increase of $S_{el}(Q)$ in that region.

The most important result is that the peak at 1.6 Å^{-1} of $S_{el}(Q)$ is not present in the inelastic structure factors. As for propagating sound waves, the inelastic structure factor $S_{\Delta\omega}(Q)$ follows approximately a $Q^2 S_{el}(Q)$ law (Buchenau *et al.* 1985); this result shows that the oxygen vibrating modes are mainly random-phase modes in this energy range.

Finally, the temperature dependence of the elastic structure factor is shown in figure 7(*a*) for the 0.8 g cm^{-3} sample; the intensity of $S_{el}(Q)$ decreases with temperature, because of the Debye–Waller factor, $\exp\{-Q^2\langle u^2\rangle\}$.

An evaluation of the mean-square displacement $\langle u^2\rangle$ can be inferred from the slope of the $\log\{S_{el}(Q,T)/S_{el}(Q,T = 100\,\mathrm{K})\}$ versus Q^2, (figure 7(*b*), where the values of $\langle u^2\rangle$ as a function of the temperature are reported). We note a linear temperature dependence, indicating harmonic behaviour only at low temperature. The deviation observed at higher temperatures has no clear origin. A possible cause

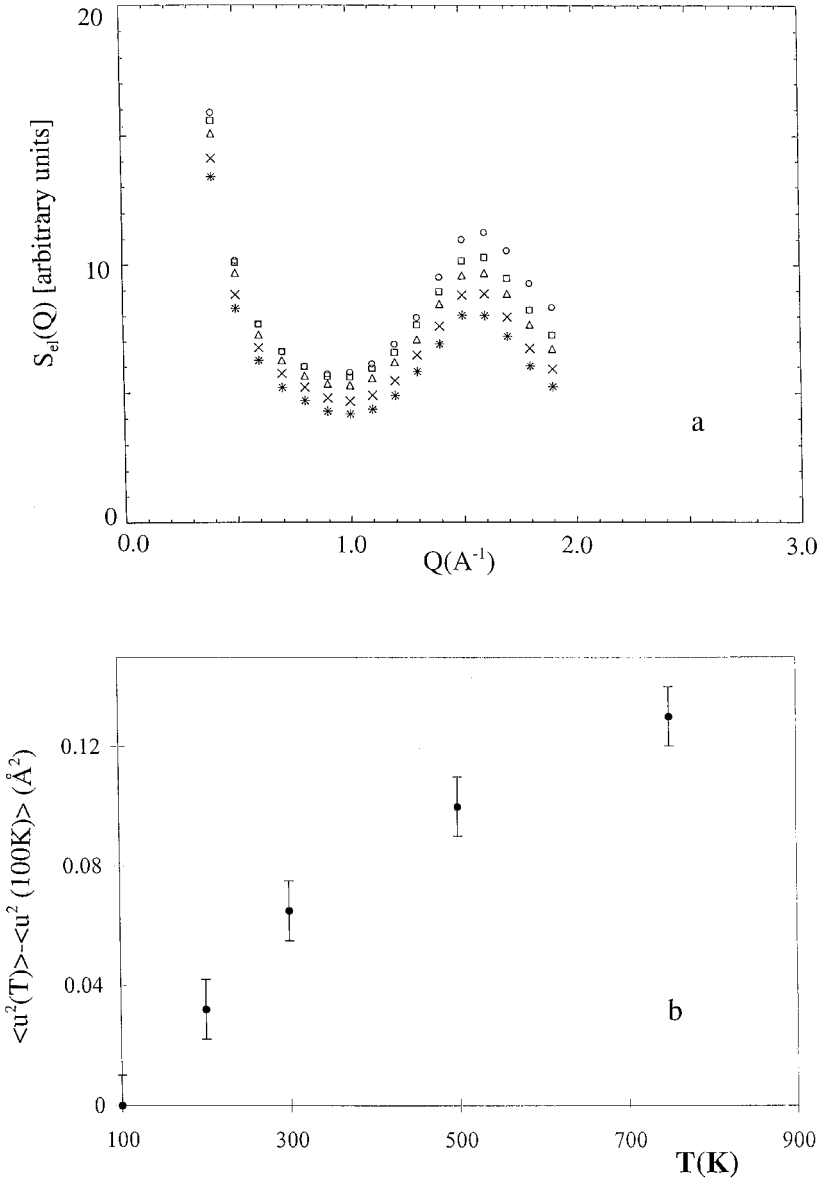

Figure 7. (*a*) Temperature dependence of the elastic structure factor for the $\rho = 0.8\,\mathrm{g\,cm^{-3}}$ xerogel: 100 K (circles), 200 K (squares), 300 K (triangles), 500 K (crosses), 750 K (stars); (*b*) temperature dependence of the mean-square displacement $\{\langle u^2(T)\rangle - \langle u^2(100\,\mathrm{K})\rangle\}$, calculated as described in the text.

could be the loss of the adsorbed water at high temperatures, since $\langle u^2 \rangle$ of water is expected to be higher than that of silica.

§ 4. Conclusions

We have found evidence for the role of water dynamics in these kinds of xerogel. In the 'dry' systems we have found, in Raman scattering, either the boson peak or a

peak at about 8–16 cm^{-1} which could be the signature of localized dynamics due to surface modes of pores. The density of states, observed by neutron scattering, is quite similar to that measured in melt quenched vitreous silica in the frequency region of the boson peak. The Q dependence of the inelastic structure factors measured in these systems at the boson peak frequency is also very similar to that measured in vitreous silica. In particular the absence of the peak at 1.6 A^{-1} in the inelastic structure factor $S(Q, \omega_{BP})$ could prove the existence of random-phase motion contributions in this frequency range.

Acknowledgements

This work is partially supported by the projects: Programma Galileo and Murst-COfin98. The authors wish to thank Professor G. Viliani for useful discussions.

References

Armellini, C., Del Longo, L., Ferrari, M., Montagna, M., Pucker, G., and Sagoo, P., 1998, *J. Sol Gel Sci. Technol.,* **13**, 599.

Brinker, C. J. and Scherer, G. W., 1990, *Sol–Gel Science* (New York: Academic Press).

Brodin, A., Fontana, A., Borjesson, L., Carini, G., and Torell, L. M., 1994, *Phys. Rev. Lett.,* **73**, 2067.

Buchenau, U., 1985, *Z. Phys.* B, **58**, 181.

Buchenau, U., Prager, M., Nucker, N., Dianoux, A. J., Ahmad, N., and Phillips, W. A., 1986, *Phys. Rev.* B, **34**, 5665.

Buchenau, U., Zhow, H. M., Nucker, N., Gilroy, K. S., and Phillips, W. A., 1988, *Phys Rev. Lett.,* **60**, 1318.

Carini, G., D'Angelo, G., Tripodo, G., Fontana, A., Leonardi, A., Saunders, G. A., and Brodin,A., 1995, *Phys. Rev.* B, **51**, 9342.

Dieudonné-George, P., 1998, thesis, University of Montpellier II. France.

Fontana A., Dell'Anna, R., Montagna, M., Rossi, F., Viliani, G., Ruocco, G., Sampoli, M., Buchenau, U., and Wischnewski, A., 1999a, *Europhys. Lett.,* **47**, 56.

Fontana, A., Montagna, M., Rossi, F., Ferrari, M., Pelous, J., Terki, F., and Woigner, T., 1999b, *J. Phys. condens. Matter,* **11**, A207.

Fontana, A., Montagna, M., Rossi F., Scopigno T., Pelous J., Terki F,. Pilliez J. N., Dieudonne, P., Cicognani, G., and Dianoux, A. J., 1999c (to be published).

Fontana, A., Rocca, F., and Fontana, M. P., 1987, *Phys. Rev. Lett.,* **58**, 503.

Fontana, A., Rossi, F., Carini, G., D'Angelo, G., Tripodo, G., and Bartolotta, A., 1997, *Phys. Rev. Lett.,* **78**, 1078.

Fontana, A., Rocca, F., Fontana, M. P., Rosi, B., and Dianoux, A. J., 1990, *Phys. Rev.* B, **41**, 3778.

Fontana, A., and Viliani, G., 1995, *Phil. Mag.* B, **71**, Special issue.

Fontana, A., and Viliani, G., 1998, *Phil. Mag.* B, **77**, 209–716.

Galenneer, F. L., and Sen, P. L., 1978, *Phys. Rev.* B, **17**, 1928.

Karpov, V. G., and Parshin, D. A., 1985, *Zh. Eksper. Teoret. Fiz.,* **88**, 2212; *Sov. Phys. JETP,* **61**, 1308.

Mariatto, G., Montagna, M., Viliani, G., Campostrini, R., and Carturan, G., 1988, *J. Phys.,* **21**, L797.

Masciovecchio, C., Mazzacurati, V., Monaco, G., Ruocco G., Scopigno, T., Sette, F., Benassi, P., Cunsolo, A., Fontana, A., Krisch, M., Mermet, A., Montagna, M., Rossi, F., Sampoli, M, Signorelli, G., and Verbeni, R., 1999, *Phil. Mag.* B, **79**, 2013.

Phillips, W. A., 1981, Low Temperature Properties: (Berlin: Springer–Verlag).

Price, D. L., and Carpenter, J. M., 1987, *J. non-crystalline Solids,* **92**, 153.

Sokolov, A. P., Kislink, A., Quitmann, D., and Duval, E., 1993, *Phys. Rev.* B, **48**, 7692.

Wischnewski, A., Buchenau, U., Dianoux, A. J., Kamitakahara, W. A., and Zaretsky, J. L., 1998, *Phil. Mag.* B, **77**, 579.